Lab on a Chip

Accepted Manuscript

ROYAL SOCIETY OF CHEMISTRY

www.rsc.org/loc

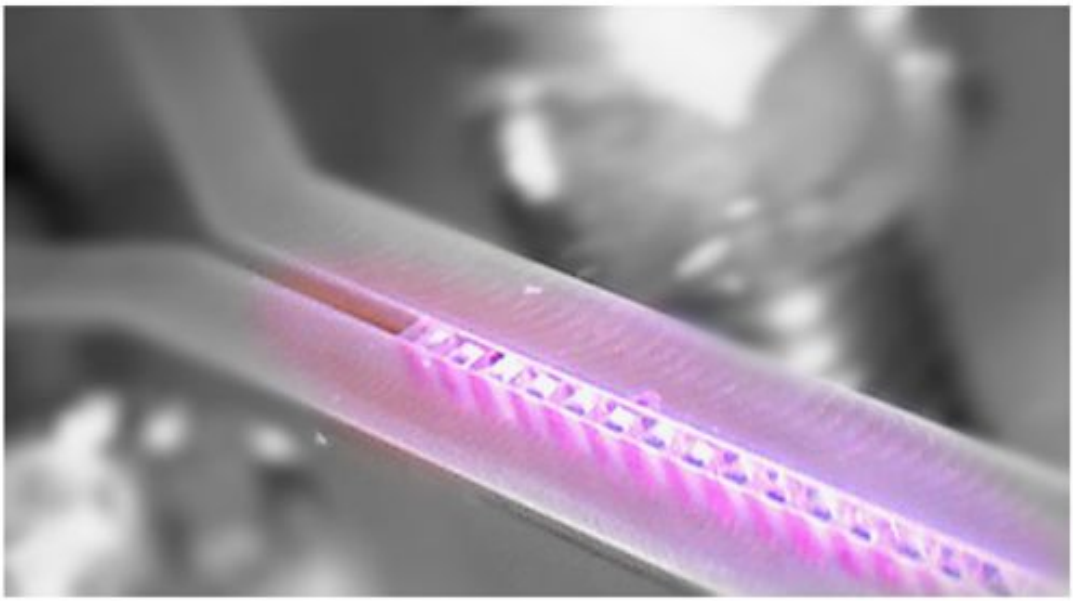

A microfluidic device is designed and used to investigate interfacial polymerization film formation in situ.

ARTICLE TYPE www. rsc.org/xxxxxx | XXXXXXXX

Visualization and characterization of interfacial polymerization layer formation†

Yali Zhang,[a] Nieck E. Benes,[b] and Rob G.H. Lammertink *[a]

Received Xth XXXXXXXXXX 20XX, Accepted Xth XXXXXXXXX 20XX
First published on the web Xth XXXXXXXXXX 200X
DOI: 10.1039/b000000x

We present a microfluidic platform to visualize the formation of free-standing films by interfacial polymerization. A microfluidic device is fabricated, with an array of micropillars to stabilize an aqueous-organic interface that allows a direct observation of the films formation process via optical microscopy. Three different amines are selected to react with trimesoyl chloride: piperazine, JEFFAMINE®D-230, and an ammonium functionalized polyhedral oligomeric silsesquioxane. Tracking the formation of the free-standing films in time reveals strong effects of the characteristics of the amine precursor on the morphological evolution of the films. Piperazine exhibits a rapid reaction with trimesoyl chloride, forming a film up to 20 μm thick within half a minute. JEFFAMINE®D-230 displays much slower film formation kinetics. The location of the polymerization reaction was initially in the aqueous phase and then shifted into the organic phase. Our in-situ real-time observations provide information on the kinetics and the changing location of the polymerization. This provides insights with important implications for fine-tuning of interfacial polymerizations for various applications.

1 Introduction

Interfacial polymerization (IP) is widely employed for the rapid production of high-selective polyamine (PA) films, and it finds intensive application in the fabrication of membranes for molecular separation.[1,2] In IP the polymerization and the film formation occur simultaneously at the interface between two immiscible solvents. Typically, an amine is dissolved in an aqueous phase and an acyl chloride is dissolved in an organic phase. The increases in thickness and density of the film that is forming inhibit the diffusion of the monomers through, and force the polymerization reaction to be self-limiting. The IP film is generally fabricated atop a porous support, by impregnating this support with an aqueous amine solution followed by immersion in an organic phase. Film thicknesses range from a few nanometer to several micrometer, depending on the monomer types and concentrations, combination of solvents, additives, and reaction times.[3–6]

The extensive application of IP films has commenced many attempts to correlate the formation kinetics to the film properties, in particular to the molecular separation performance.[3,7–10] However, the extremely rapid kinetics, and potentially changing characteristics of the film formation process in time, complicate both computational and experimental studies. Enkelmann and Wegner[8] developed the very first model considering film formation to be dictated by concurrent diffusion and reaction limitations. Since then many other studies have been focused on interfacial polymerization, aiming at finding relations between film formation kinetics and film properties such as the film thickness, polymer weight and charge distribution.[11–16] An extensive review of such models is given by Berezkin.[17] The various models range from simple phenomenological approaches to detailed molecular dynamics. In the most recognized models the film formation is considered to be a multistage processes: firstly incipient film formation occurs, followed by a slow-down of the polymerization reaction to a fully diffusion limited film growth. These models are referred to as 'double-layer model', as the film formed by the multi-stage process consists of a selective dense layer atop by a more loose layer.

Experimental studies also have revealed that the physicchemical properties of IP films vary with location inside the films.[4,7,8,18] Quantitative prediction of these variations has proven to be complicated, and also generic film property-performance relations have not yet been established. Despite that the occurrence of dual regions in IP films has also been observed frequently in experimental studies, a generic quantitative prediction of the properties of these regions remains to be challenging.

Several reviews can be found on experimental IP stud-

† Electronic Supplementary Information (ESI) available: [details of any supplementary information available should be included here]. See DOI: 10.1039/b000000x/

[a] *Soft Matter, Fluidics and Interfaces, MESA+ Institute for Nanotechnology, Faculty of Science and Technology, University of Twente, Enschede, the Netherlands. Fax: +31 53 489 2882; Tel: +31 53 489 4798; E-mail: r.g.h.lammertink@utwente.nl*
[b] *Inorganic Membranes, MESA+ Institute for Nanotechnology, Faculty of Science and Technology, University of Twente, Enschede, the Netherlands.*

ies.[1,2,19,20] These studies have not included in-situ analysis techniques that allow direct visualization of the film formation process, for validating the modeling work. Most film formation kinetics have been investigated by monitoring the reactant consumption and/or the film thickness in time, for various preparation conditions. Real-time IP film formation has mostly been investigated within the context of microencapsulation formation.[4,14,21–23] Yadav et al.[21] has succeeded in accessing the monomer consumption in the aqueous phase by employing an on-line pH probe. Chai et al.[4] has tracked the film thickness in time by using light reflection and pendant-drop tensiometry. They have confirmed that the kinetics of their process were diffusion-controlled. These techniques have limitations in the assessment of the formation process of supported and/or free-standing IP films.

In addition to the kinetics of film formation, the film properties are expected to be affected by the location of the reaction. Generally the reaction is thought to occur in the organic phase, due to the rapid hydrolysis of acid chloride in water and the asymmetric solubility of the reactants between both phases.[7,23,24] Scanty experimental real-time observations of the location of film formation have been revealed due to the lack of in-situ techniques. Observations of penetration of the IP film into the porous support imply that the reaction can occur in the aqueous phase.[25,26]

Here we attempt to establish a system that enables to track the kinetics of free-standing IP film formation, and to visualize the reaction location. Such a system can be used to address these questions by employing a microfluidic platform. The design of the microchips comprises an array of pillars inside the microchannels, allowing adequate stabilization of the aqueous-organic interface. The controlled stabilization of the liquid-liquid interface at designated position enables visualizing the film formation process in-situ, providing information on the evolution of the kinetics and the location of the polymerization reaction.

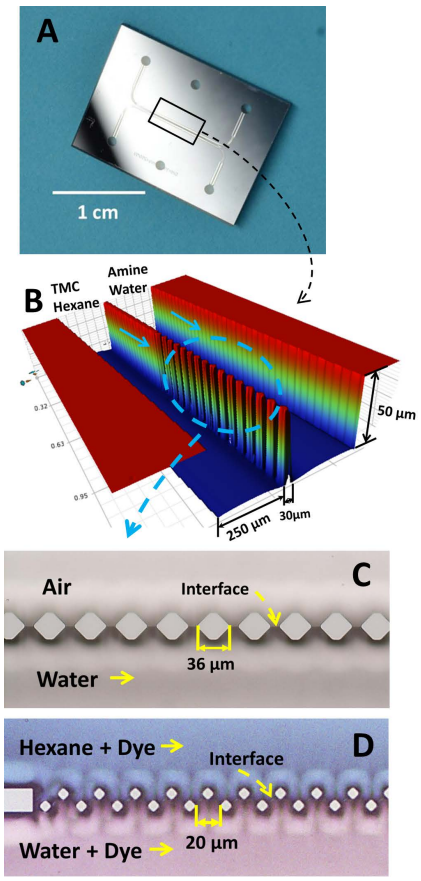

Fig. 1 (A) Silicon-Glass bonded microchip for IP membrane formation. (B) White light interferometer image of a 3D microfluidic configuration 1 with hexagon-shaped subchannel. (C) Optical microscopy image of a stable gas-aqueous interface control by configuration 1. (D) Optical microscopy image of a stable organic-aqueous interface control at a zigzag-shaped subchannel in configuration 2.

2 Experiments

2.1 Microchips

The microchannels were fabricated on a silicon wafer by standard photolithography followed with deep reactive ion etching. The silicon wafer was anodically bonded to a glass wafer (Figure 1 (A)). The bonded chip was enclosed to a tailor-made chip holder and connected (Upchurch connections) to elevated reservoirs for flow control.

2.2 Interfacial polymerization membrane formation

Before the interfacial polymerization reaction, the inner walls of the microchannels were chemically hydrophobized by silicon oil (20 cSt, Sigma-Aldrich).[27] Three amine solutions were prepared at 0.5 wt% in deionized water: piperazine (PIP, Sigma-Aldrich), JEFFAMINE®D-230 (JEFF, Huntsman), and a hybrid polyhedral oligomeric silsesquioxane (POSS, Hybrid Plastics). Sodium hydroxide (Sigma-Aldrich) was added to the ammonium functionalized POSS solution.[28] An amine solution was introduced into one of the main channels by providing a hydrostatic pressure of 2400 Pa (Δh=240 mm). The micropillars provided adequate pinning sites to stabilize the G-L interface (Fig. 1 (C)). After the G-L interface was stable, the outlet of the aqueous solution was blocked to equalize the pressure in the microchannel and create a stationary aqueous-G interface. Upon that, a trimesoyl chloride (TMC, Sigma-Aldrich) in hexane solution (0.25 wt%, Sigma-Aldrich) was flowed into the adjacent channel by another hydrostatic head. The offered pressure (Δh=100 mm)

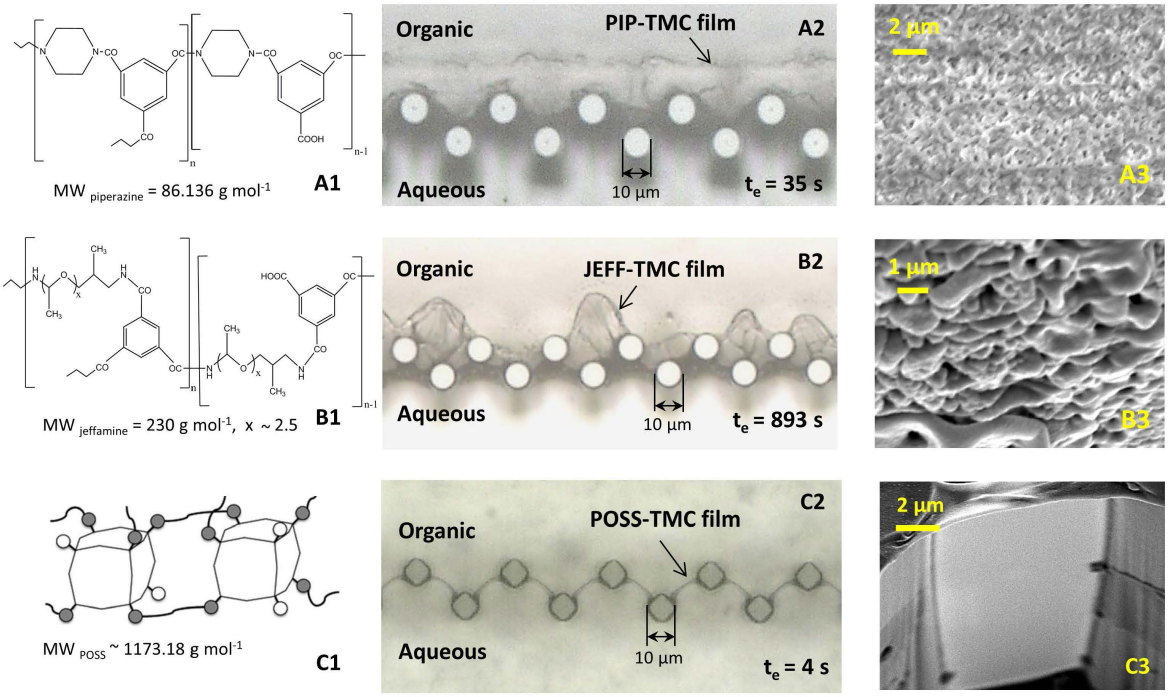

Fig. 2 IP film morphologies from the top-view of the microchannel formed by different aliphatic amines reacted with TMC. The left column shows the reaction schemes and the molecular weights (MW) of the corresponding monomers. The middle column are the microscopy images of the formed IP films in configuration 2. The right column are the SEM images of the corresponding micro-IP films.

was just sufficient to drive in the organic solution to minimize the caused instability on the formed L-L interface. Once the interface was formed, the reaction was ensured to occur under a free-pressure-driven condition by opening all the connections to the air. The IP film formation was recorded using a high-speed camera (AxioCam MRc 5, Carl-Zeiss) connected to the optical microscope (Axiovert 40, Carl-Zeiss). Pure water and hexane were flowed into the corresponding channels to remove unreacted monomers after the formation process was completed.

2.3 Scanning Electron Microscope (SEM) samples preparation

We employed two methods to prepare SEM samples regarding the film properties. Samples of PIP and JEFF films were prepared by dissolving the covered glass slide in 50% HF acid for 70 min under an etching rate of 7 μm min^{-1}. Thermal bonded devices (see SI.1) could be separated by mechanical force, after the POSS film formation.

2.4 Water permeation measurements

The water permeability of the POSS-TMC film was analyzed by providing a constant feed pressure using hydrostatic heads. Hexane and DI water were firstly flowed into the main channel synchronously. The outlet of the water stream was blocked to equalize the pressure in the water-filled channel. The inlet and outlet of the hexane filled channel were opened to the atmosphere. A hydrostatic pressure difference of 3500 Pa (Δh=350 mm) was applied to the water stream. Permeating water droplets in the hexane phase were recorded by a camera. The droplet sizes were analyzed using the program ImageJ (Version 1.46). The water permeability was calculated from the change in droplet dimensions.

3 Results and discussion

The design of our microfluidic devices features two parallel channels, allowing the simultaneous flows of an aqueous and an organic stream. An array of micropillars (Fig. 1 (A) and (B)) stabilizes the interface between the liquids, and provides mechanical support for the film that is formed at this interface. We have designed various pillar structures to optimize the L-L interface control and investigate their influences on the film formation process (see SI.2). The hexagon-shaped pillar (configuration 1, Fig. 1(C)) and the zigzag-located pillar (Configuration 2, Fig. 1(D)) provide well-stabilized interfaces and have been selected for this study. All the IP formation

experiments were performed in configuration 2. This configuration offers the largest interfacial areas, which facilitates the microscopic observation. Configuration 1 was utilized for water permeation measurements as this configuration reduces the coalescence of growing water droplets.

We selected three different amines to react with TMC: PIP, JEFF and POSS. PIP is one of the most widely used aliphatic amines for the fabrication of nanofiltration and reverse osmosis membranes by IP. Its derived IP films typically exhibit a large free volume and pore size, enabling a high permeability.[10,29] JEFF is a polyetheramine with long and flexible aliphatic chains. It has been scarcely selected as an amine candidate for IP film formation, due to the long flexible alkyl chains that result in an even larger free volume as compared to PIP. Films with a very open structure generally exhibit low salt retentions. POSS has recently drawn tremendous attention due to its unique hybrid structure. Supported POSS membranes exhibit an extremely dense morphology and thin thickness (<300 nm) providing extraordinary performance for gas and liquid permeation applications.[30,31]

Figure 2 (A) and (B) reveal the morphologies of films prepared with the two aliphatic amines. The reaction between PIP and TMC is fast, resulting in the formation of a $\sim 20\ \mu$m film in the hexane phase, within 30 s (Fig. 2 (A2)). The direction of film growth implies that the reaction predominantly takes place in the organic phase. The optical microscopy image shows that the cross sectional morphology of the film does not vary strongly with axial position. The SEM micrograph of the film surface at the hexane side (Fig. 2 (A3)) reveals some roughness. Such roughness has also been typically reported for IP formation of supported PIP films.[10,18] Figure 2 (B2) depicts a film obtained with JEFF as amine source. The film consists of a stack of two regions: a $\sim 5\ \mu$m dense region in between the pillars, and a more loose and irregular region up to 25 μm towards the organic phase. The SEM image (Fig. 2 (B3)) confirms that surface of the film on the organic side is rougher as compared to the PIP derived film.

It is noted that the thicknesses of the free-standing PIP and JEFF films are up to ten times thicker than those of supported films. Similar differences between supported and free-standing films have also been reported by others.[4,8] The differences can be related to a more limited amount of amines available for the reaction in the case of an impregnated support, and mechanical stabilization of the liquid-liquid interface by the porous support.

Exploiting our microfluidic platform, the film formation process can be traced in time. Figure 3 reveals the evolution of film formation for the polymerization of JEFF with TMC. Initially, a thin JEFF film is formed instantly as the interface is generated (Fig. 3 (A)). The positions of the initial interface and its adjacent three pillars are highlighted in red (Fig. 3 (A1)-(E2)). The growth direction and thickness in time can be

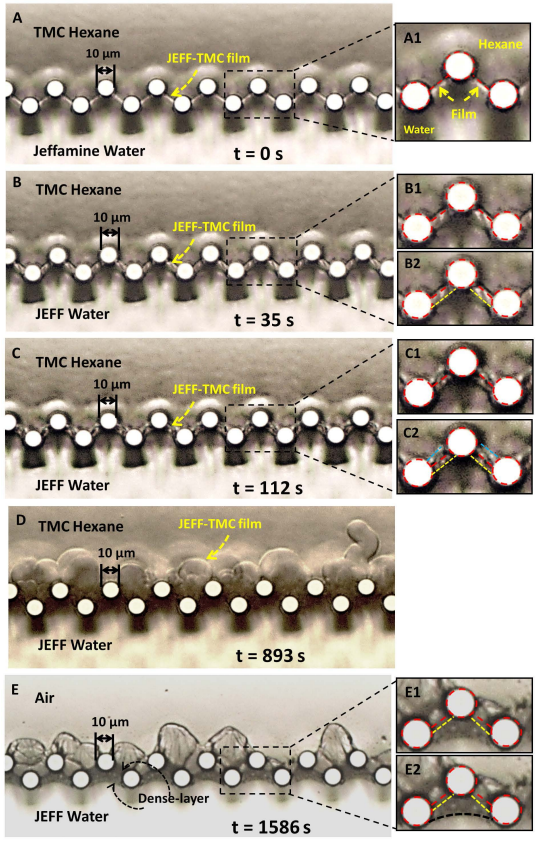

Fig. 3 Optical microscopy images of JEFF-TMC film formation process. (A) (E) JEFF IP film formation at different time steps. (E) The JEFF IP film morphologies after drying the hexane phase. (A1)-(E1) Highlighted initial film position and adjacent pillars. (B2)-(E2) Highlighted film-liquid interface in different time steps (Yellow: film/aqueous interface at t=35 s. Blue: film/organic interface at t=112s. Black: film/aqueous interface after the reaction is complete).

determined by measuring the deviation of the film/liquid interface from the initial interface (SI.2). At 35 s, a film has been formed with an average thickness of $\sim 2\ \mu$m in the aqueous phase (the film/aqueous interface is indicated in yellow), and a thickness of less than 1 μm in the organic phase (Fig. 3 (B2)). Such growth implies that, initially, the polymerization reaction predominantly occurs in the aqueous phase, instead of in the organic phase. This is distinct from observations for PIP (Fig. SI(2)). The different initial behavior can be rationalized from the difference in distribution of the amines over the two liquid phases; the more hydrophilic JEFF has a lower tendency to go into the organic phase as compared to PIP. For JEFF, after 112 s the thickness of the film grown into the organic phase has increased to $\sim 3\ \mu$m, while no apparent further growth into the aqueous phase is observed (Fig. 3 (C2)). This indicates

that the formed film possesses an increased mass transport resistance for TMC that localizes the reaction into the organic phase. Up to 112 s, the growth of the film has resulted in a homogenous thickness, and the film only grows perpendicularly from the incipient layer. Upon that, the JEFF film further grows into the hexane phase in more irregular fashion. After approximately 900 s no apparent further growth of the film is observed. Meanwhile, the reaction in the aqueous solution has proceeded at a low rate, as is manifested by a slight shift of the interface between films and aqueous solution (Fig. 3 (E2)).

Differently from PIP and JEFF, POSS established a more homogeneous film in terms of thickness and morphology between adjacent pillars (Fig. 2 (C2)). The obtained film thickness is thinner than 300 nm, which is approximately twice thicker that of the supported analogue.[28] By tracking the formation of POSS IP film in time, we observed no apparent growth of film thickness and density after 4 s (4 s was the minimal time step we used). We presume that the huge POSS molecule tends to form a dense film (Fig. 2 (C3)), and the transport of POSS through the forming film is instantly obstructed. The reaction is unable to proceed in the water phase due to the hydrolysis of the acid chloride group of TMC. Therefore, the film formation is self-limited within such a short time. The POSS film is not only very thin, on both the organic and aqueous side of the membrane a very smooth surface is observed in the SEM images in Fig. 4 (B1) and (B2). In contrast, the JEFF derived film shows a slightly rougher surface on the aqueous side, and a very much rougher surface on the organic side. A similar correlation between film thickness and surface morphology, when comparing different amine monomers, has also been observed for supported membranes.[10]

Compared to the morphologies of POSS and PIP films, the JEFF film shows a rougher surface in the hexane phase. The flexible aliphatic chain of JEFF molecular tends to form a film with an open, gel-like or high swollen structure. A lower reactivity of JEFF with TMC compared to that of PIP, can be assumed by correlating the reaction time to the formed film thickness (30 min for $\sim 20\ \mu$m). The swollen nature and slow formation process of the JEFF films could explain the rougher surface compared to PIP and POSS films.[3]

We conducted a facile test to measure the water permeability of the free-standing POSS IP films. After around 1500 s a series of regular shaped water droplets are formed in the hexane phase (Fig. 5 (A)) that continue to grow in time. The small variation in the size of the droplets indicates that the permeance of the film is similar at all locations in the array of pillars. From the change in the projected dimensions of the droplets their volume is calculated, assuming a spherical shape. The derivative of the volume with respect to time is converted to the water permeability, which is on the order of 10 L m^{-2} h^{-1} bar^{-1}. This is about 30 times higher than that reported for the

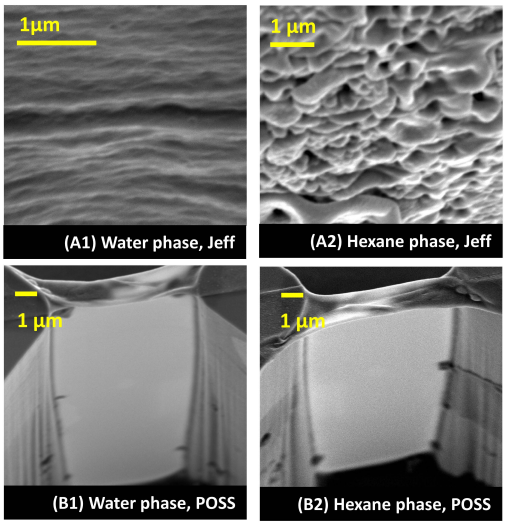

Fig. 4 SEM images of membrane morphologies at both aqueous and hexane phase. (A) is jeffamine (jeff) - TMC membrane and (B) is POSS - TMC membrane.

polyacrylonitrile (PAN) supported POSS films.[28] A relative lower water flux of IP films is obtained when a hydrophobic support is employed.[32] The absence of a hydrophobic PAN support as well as morphological differences, may cause the higher water permeability of the free-standing POSS film compared to those of the supported ones.

4 Conclusion

In conclusion, our microfluidic device allows a direct visualization of the IP film formation process. The amine monomer is proved to play a decisive role in the resulting film morphologies. We observe three different scenarios of IP film formation processes. PIP exhibits a rapid reaction with TMC and the reaction only occurs in the organic phase. JEFF tends to form a film in both aqueous and organic phases. The POSS IP film is approximately 300 nm thin and the reaction is terminated within seconds. Our in-situ real-time observations of the interfacial film formation generate information on the kinetics as well as on the evolution of the reaction location. This provides insights that may have import implications for sensible fine-tuning of interfacial polymerization for various applications.

5 Acknowledgments

The authors would like to acknowledge the Dutch technology Foundation STW for the financial support. We would like to thank S. Schlautmann (University of Twente) for the technical

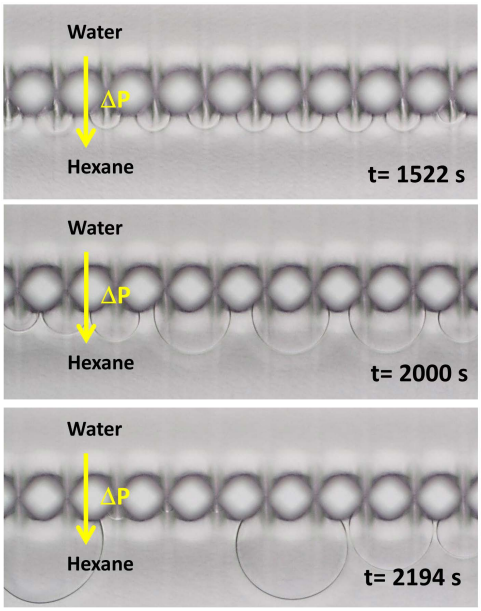

Fig. 5 Optical images of the POSS membrane for water permeation at different time steps.

support in the cleanroom, M. Raaijmakers for providing the POSS solution and K. Tempelman for the experimental assistance.

References

1 R. J. Petersen, *J. Membr. Sci.*, 1993, **83**, 81–150.
2 J. E. Cadotte, R. S. King, R. J. Majerle and R. J. Petersen, *J. Macromol. Sci., Part A: Pure Appl. Chem.*, 1981, **15**, 727–755.
3 J. Jegal, S. G. Min and K.-H. Lee, *J. Appl. Polym. Sci.*, 2002, **86**, 2781–2787.
4 G.-Y. Chai and W. B. Krantz, *J. Membr. Sci.*, 1994, **93**, 175–192.
5 C. Kong, T. Shintani, T. Kamada, V. Freger and T. Tsuru, *J. Membr. Sci.*, 2011, **384**, 10–16.
6 R. Shenoy and C. N. Bowman, *Biomaterials*, 2012, **33**, 6909–14.
7 P. W. Morgan and S. L. Kwolek, *J. Poly. Sci.*, 1959, **XL**, 299–327.
8 G. W. V. Enkelmann, *Makromol. Chem.*, 1976, **177**, 3177–3189.
9 C. Kim, J. Kim, I. Roh and J. Kim, *J. Membr. Sci.*, 2000, **165**, 189–199.
10 S. Veríssimo, K.-V. Peinemann and J. Bordado, *J. Membr. Sci.*, 2006, **279**, 266–275.
11 J. Ji, J. M. Dickson, R. F. Childs and B. E. Mccarry, *Macromolecules*, 2000, **33**, 624–633.
12 V. Freger and S. Srebnik, *J. Appl. Polym. Sci.*, 2003, **88**, 1162–1169.
13 V. Freger, *Langmuir*, 2005, **21**, 1884–1894.
14 K. Bouchemal, F. Couenne, S. Brianc, H. Fessi and M. Tayakout, *AIChE J.*, 2006, **52**, 2161–2170.
15 R. Nadler and S. Srebnik, *J. Membr. Sci.*, 2008, **315**, 100–105.
16 R. Oizerovich-Honig, V. Raim and S. Srebnik, *Langmuir*, 2010, **26**, 299–306.
17 A. V. Berezkin and A. R. Khokhlov, *J. Polym. Sci., Part B: Polym. Phys.*, 2006, **44**, 18–20.
18 V. Freger, *Langmuir*, 2003, **37**, 4791–4797.
19 Y. Song, P. Sun, L. Henry and B. Sun, *J. Membr. Sci.*, 2005, **251**, 67–79.
20 W. Lau, a.F. Ismail, N. Misdan and M. Kassim, *Desalination*, 2012, **287**, 190–199.
21 S. K. Yadav, A. K. Suresh and K. C. Khilar, *AIChE J.*, 1990, **36**, 431–438.
22 S. K. Karode, R. S. S. Kulkarni, A. K. S. Suresh and R. A. Mashelkar, *Chem. Eng.Sci*, 1997, **52**, 3243–3255.
23 S. Dhumal, S. Wagh and a. Suresh, *J. Membr. Sci.*, 2008, **325**, 758–771.
24 S. a. Sundet, *J. Membr. Sci.*, 1993, **76**, 175–183.
25 C. R. Bartels, K. L. Kreuz and A. Wachtel, *J. Membr. Sci.*, 1987, **32**, 291–312.
26 C. R. Bartels, *J. Membr. Sci.*, 1989, **45**, 225–245.
27 R. Arayanarakool, L. Shui, A. van den Berg and J. C. T. Eijkel, *Lab. Chip*, 2011, **11**, 4260–6.
28 M. Dalwani, J. Zheng, M. Hempenius, M. J. T. Raaijmakers, C. M. Doherty, A. J. Hill, M. Wessling and N. E. Benes, *J. Mater. Chem.*, 2012, **22**, 14835.
29 F. Yang, S. Zhang, D. Yang and X. Jian, *J. Membr. Sci.*, 2007, **301**, 85–92.
30 M. J. T. Raaijmakers, M. A. Hempenius, P. M. Schön, G. J. Vancso, A. Nijmeijer, M. Wessling and N. E. Benes, *J. Am. Chem. Soc.*, 2014, **136**, 330–5.
31 M. L. Chua, L. Shao, B. T. Low, Y. Xiao and T.-S. Chung, *J. Membr. Sci.*, 2011, **385-386**, 40–48.
32 J. R. McCutcheon and M. Elimelech, *J. Membr. Sci.*, 2008, **318**, 458–466.